

# Bright stars observed by FIMS/SPEAR

Young-Soo Jo,<sup>1,2\*</sup> Kwang-II Seon,<sup>1,3</sup> Kyoung-Wook Min,<sup>2</sup> Yeon-Ju Choi,<sup>2,4</sup>  
Tae-Ho Lim,<sup>2</sup> Yeo-Myeong Lim,<sup>2</sup> Jerry Edelstein,<sup>5</sup> and Wonyong Han<sup>1</sup>

<sup>1</sup>Korea Astronomy and Space Science Institute (KASI), 776 Daedeokdae-ro, Yuseong-gu, Daejeon, Korea 305-348, Republic of Korea

<sup>2</sup>Korea Advanced Institute of Science and Technology (KAIST), 291 Daehak-ro, Yuseong-gu, Daejeon, Korea 305-701, Republic of Korea

<sup>3</sup>Astronomy and Space Science Major, Korea University of Science and Technology, 217 Gajeong-ro, Yuseong-gu, Daejeon, Korea 305-350, Republic of Korea

<sup>4</sup>Korea Aerospace Research Institute (KARI), 169-84 Gwahak-ro, Yuseong-gu, Daejeon, Korea 305-806, Republic of Korea

<sup>5</sup>Space Sciences Laboratory, University of California, Berkeley, CA, USA

1 June 2021

## ABSTRACT

In this paper, we present a catalogue of the spectra of bright stars observed during the sky survey using the Far-Ultraviolet Imaging Spectrograph (*FIMS*), which was designed primarily to observe diffuse emissions. By carefully eliminating the contamination from the diffuse background, we obtain the spectra of 70 bright stars observed for the first time with a spectral resolution of 2–3 Å over the wavelength of 1370–1710 Å. The far-ultraviolet spectra of an additional 139 stars are also extracted with a better spectral resolution and/or higher reliability than those of the previous observations. The stellar spectral type of the stars presented in the catalogue spans from O9 to A3. The method of spectral extraction of the bright stars is validated by comparing the spectra of 323 stars with those of the International Ultraviolet Explorer (*IUE*) observations.

**Key words:** catalogues – ultraviolet: stars – stars: general – instrumentation: spectrographs – methods: data analysis – techniques: spectroscopic

## 1 INTRODUCTION

Among the space missions that have observed stellar spectra in the range of the far ultraviolet (FUV) wavelength, the International Ultraviolet Explorer (*IUE*; Boggess et al. 1978) has the most extensive list of targets with approximately 5,000 stars with their spectra taken for the wavelength range of 1150–1980 Å with a resolution of 0.1–0.3 Å. Although the wavelength coverage might differ slightly among various missions, there have been a number of additional small and full-scale missions. These include the S2/68 Ultraviolet Sky Survey Telescope (*UVSST*; Boksenberg et al. 1973; Jamar et al. 1976) aboard the ESRO Satellite TD-1, Copernicus (Rogerson et al. 1973; Snow & Jenkins 1977), *SKYLAB* Experiment S-019 (Henize et al. 1975, 1979), Hopkins Ultraviolet Telescope (*HUT*; Davidsen et al. 1992; Kruk et al. 1995), Orbiting Retrievable Far and Extreme Ultraviolet Spectrometers (*ORFEUS*; Jenkins et al. 1996), Far Ultraviolet Spectroscopic Explorer (*FUSE*; Moos et al. 2000; Sahnou et al. 2000), Galaxy Evolution Explorer (*GALEX*; Morrissey et al. 2007; Bertone & Chavez 2011), and Space Telescope Imaging Spectrograph (*STIS*; Woodgate et al. 1998 and *StarCAT*; Ayres 2010), Goddard High Resolution Spectrograph (*GHRS*; Brandt et al. 1994), Cosmic Origins Spectrograph (*COS*; Green et al. 2012) aboard the Hubble Space Telescope (HST). As a result of these ob-

servations, the spectra of approximately 10,000 stars are now available in the FUV wavelengths.

Recently, the Far-Ultraviolet Imaging Spectrograph (*FIMS*), also known as the Spectroscopy of Plasma Evolution from Astrophysical Radiation (*SPEAR*), performed an all-sky survey in the FUV wavelength region. The *FIMS* is a dual channel imaging spectrograph (*S*-band: 900–1150 Å, *L*-band: 1370–1710 Å) with moderate spectral ( $\lambda/\Delta\lambda \sim 550$ ) and angular ( $\sim 5'$ ) resolutions, and it was designed for the observation of diffuse emissions from interstellar medium (Edelstein et al. 2006a,b). The primary purpose of the *FIMS* is to study the FUV emission from atomic, ionic, and molecular species in a variety of interstellar environments (e.g. Korpela et al. 2006). In addition, a number of bright stars have also been observed when they are within its large image fields of view, defined by the slit size (*S*-band:  $4^\circ 0 \times 4' 6$ , *L*-band:  $7^\circ 5 \times 4' 3$ ). This paper discusses the spectral extraction of these observed bright stars.

The *FIMS* was used to make observations for one and a half years, covering more than 80% of the sky, after its launch by the Korean microsatellite *STSAT-1* on 27 September 2003 into a 700 km sun-synchronous orbit. Although stars were observed in both the *S*- and *L*-bands, the *S*-band data were excluded from the present analysis because of their strong contamination with geocoronal emission lines as well as the low detector sensitivity. We extracted the *L*-band spectra for 532 stars from 1,523 orbits of observations during its mission lifetime, from which 70 stars were observed for the first time. Here, we report the FUV spectra of these stars along

\* E-mail: stspeak@kasi.re.kr

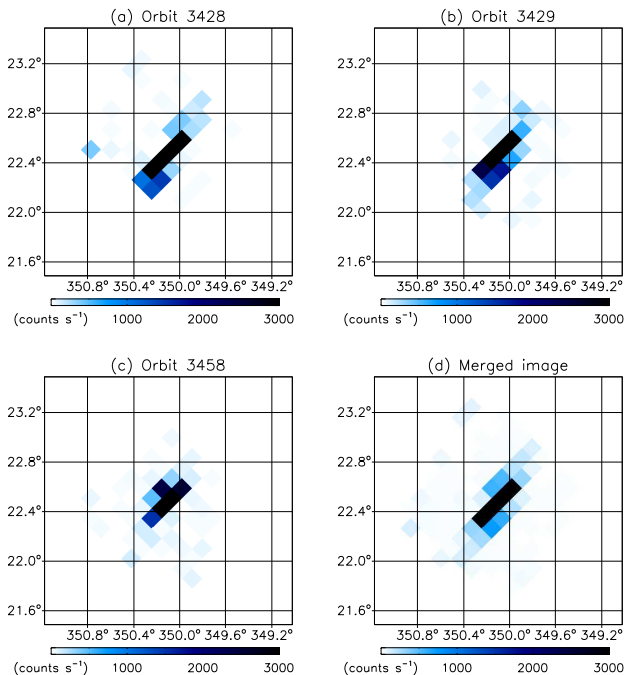


**Figure 1.** Photon count-rate (unit:  $\text{count s}^{-1}$ ) images of HD 143275 with Galactic coordinates: the multiple images of (a) to (c) are merged into one, as shown in (d).

with those of the 139 stars that were observed with a better spectral resolution and/or higher reliability than those of the previous observations, as the *FIMS* catalogue stars. The remaining 323 stars, which were also observed by the *IUE* in a large aperture mode, were used to validate the *FIMS* spectra. Most of the 323 stars were observed in the high-dispersion mode of the *IUE* with a spectral resolution of  $\sim 0.2 \text{ \AA}$ , but 34 stars among them were observed in the low-dispersion mode and with a lower spectral resolution of  $\sim 6 \text{ \AA}$ . Section 2 describes the data processing steps used to obtain the FUV spectra of the observed stars, and Section 3 presents the detailed descriptions of the statistical properties of the *FIMS* catalogue stars. A summary is provided in Section 4.

## 2 DATA PROCESSING STEPS

We followed three key steps to obtain the spectral information of the stars that were observed with a diffuse background. A detailed description about flat-fielding as well as the procedures of wavelength and flux calibration for the *FIMS* data can be found in Edelstein et al. (2006b). In the present paper, we report only on the process of spectral extraction of bright stars from the existing *FIMS* archival data. However, the new effective area was derived as it was seen to change significantly over the mission time due to degradation in detector sensitivity (Section 2.3).

### 2.1 Step 1: Identification of stars and merging of data

The *FIMS* data, which were archived in the FITS format with coordinates and wavelengths assigned to each photon, were arranged to form an image tile for each orbit of observations and pixelated using the HEALPIX scheme (Gorski et al. 2005) with a resolution

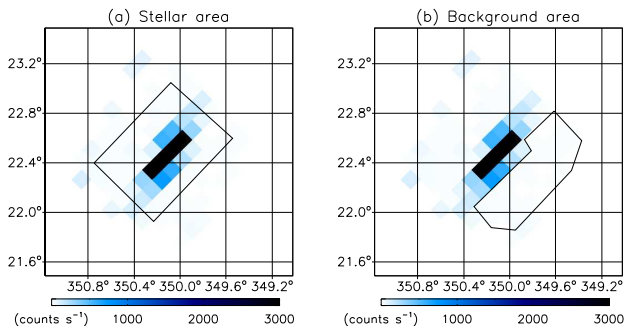


**Figure 2.** Stellar and background areas selected for HD 143275 are presented in the left and right panels, respectively.

parameter of  $N_{\text{side}} = 512$ , corresponding to a pixel size of approximately 7 arcmin. The constant pixel area of the HEALPIX scheme makes it convenient to extract stellar spectra, which are mixed with the background spectra because of instrumental scattering.

We identified the stars by comparing the *FIMS* images with the locations of the bright stars in the *TDI* star catalogue (Thompson et al. 1978) based on the S2/68 Ultraviolet Sky Survey Telescope (*UVSST*) of the *TDI* satellite. *UVSST* is described in Boksenberg et al. (1973) and the absolute calibration of the instrument is given in Humphries et al. (1976). *UVSST* consisted of an  $f/3.5$  telescope with a primary mirror having a diameter of 27.5 cm, feeding photons to a spectrometer and photometer. The spectrometer has an entrance aperture of  $11.8 \times 17'$  and a wavelength band in the range of 130–255 nm with spectral resolution of 35  $\text{\AA}$ . The photometer has an aperture of  $1.7 \times 17'$  with a broad passband (31 nm) centred at 274 nm. The first *UVSST* spectral catalogue for 1,356 stars was published by Jamar et al. (1976)<sup>1</sup>. Later, Thompson et al. (1978)<sup>2</sup> extended the catalogue to 31,215 stars and provided the absolute UV fluxes in four passbands: 135–175 nm, 175–215 nm, 215–255 nm, and the photometric band at 274 nm. The fluxes of the first three wavelength bands were obtained by binning the spectrophotometric data, and the flux of the longest wavelength band was based on the photometric data only. Hence, the angular resolution of the catalogue is limited by that of the photometer, which is 2 arcmin. It is notable that the shortest passband of 135–175 nm, centred at 1565  $\text{\AA}$  (henceforth, F1565), is comparable with that of the *FIMS* *L*-band and was used for identification of UV bright stars in the present study because the *TDI* is more sensitive and has higher angular resolution than *FIMS*. We note that the photometric catalogue (henceforth, *TDI*) extended by Thompson et al. (1978) were used to identify stars, while the spectral catalogue (henceforth, *UVSST*) made by Jamar et al. (1976) were used to compare with the *FIMS* spectra after Section 3.

In order to avoid misidentification of stars in crowded areas and contamination by other bright stars in the surrounding region, we selected only the stars listed in the *TDI* catalogue that were isolated within the  $2^\circ \times 2^\circ$  angular region centred around the target stars. Since the angular resolution of *TDI* ( $2'$ ) is higher than that of the *FIMS*, we believe that the *TDI* catalogue is able to resolve the stars even for those that the *FIMS* cannot if the stars were bright enough to be observed by *TDI*. Hence, the angular resolution of the *FIMS* catalogue is limited by that of the *TDI* catalogue. Further, we checked the  $2^\circ \times 2^\circ$  *FIMS* images and discarded the pixels

<sup>1</sup> <http://vizier.u-strasbg.fr/viz-bin/VizieR?-source=III/39A>

<sup>2</sup> <http://vizier.u-strasbg.fr/viz-bin/VizieR?-source=II/59>

**Table 1.** List of the *IUE* reference stars, together with the orbit number and the dates of the *FIMS* observations.

HD ID	Orbit	Observational date	HD ID	Orbit	Observational date
21790	1116	2003-12-12	100889	2559	2004-03-20
46487	1254	2003-12-21	83058	2561	2004-03-20
32249	1292	2003-12-24	79447	2772	2004-04-03
31726	1341	2003-12-27	98718	2973	2004-04-17
25340	1455	2004-01-04	105937	3053	2004-04-22
68217	1929	2004-02-05	108257	3054	2004-04-22
63922	1964	2004-02-08	152614	3610	2004-05-30
64740	1994	2004-02-10	158094	3847	2004-06-16
70556	2006	2004-02-11	165024	3947	2004-06-22
64802	2057	2004-02-14	166182	3955	2004-06-23
76566	2070	2004-02-15	172910	4061	2004-06-30
75821	2075	2004-02-15	207971	4639	2004-08-09
67797	2078	2004-02-16	188665	5226	2004-09-18
76805	2443	2004-03-12	207330	5635	2004-10-16

brighter than the background median values by a factor of three, except those associated with the target stars. The faintest star in the resulting *FIMS* catalogue has a flux of  $\sim 7 \times 10^{-12}$  erg s $^{-1}$  cm $^{-2}$  Å $^{-1}$ , much higher than the typical *TDI* flux limit of  $10^{-12}$  erg s $^{-1}$  cm $^{-2}$  Å $^{-1}$  in the spectral band of 1350–1750 Å. Although we avoided regions of high concentration of UV sources on the basis of the *TDI*, there may still exist some stars which were not resolved in the *TDI* catalogue among the *FIMS* catalogue stars. However, we found no bright stars near the stars included in the *FIMS* catalogue. Instead, some stars that were observed by *FIMS* but not included in our catalogue were found to be contaminated by unresolved stars. For example, HD 214167 (B1.5Vs; Abt & Cardona 2011) was found to form a double system with one of the *FIMS* star of HD 214168 (B1Vne; Abt & Cardona 2011), separated by an angular distance of  $\sim 0.37'$ . As another example, HD 199739 with a spectral type of B2II (Hill & Lynas-Gray 1977) was found at an angular distance of  $4'$  from one of the *FIMS* star of HD 199661. However, the star is fainter than HD 199661 by 1.7 mag (21%) in V band and 2.8 mag (8%) in U band (Reed 2003). These two stars were not included in the *FIMS* catalogue since they were also observed by the *IUE*. In summary, although the  $2^\circ \times 2^\circ$  angular region may contain many other stars not resolved in the *TDI*, the contamination due to them would not be significant.

Once the target star was identified and the region of  $2^\circ \times 2^\circ$  tiles were confirmed to be free of bright stars, we performed a Gaussian fitting for each image to find the centre of the star. We note that instrumental scattering results in diffuse images even for a point source. The selection of this large area around each star is necessary because the instrumental scattering by the slit caused the elongated image of a bright star along the slit direction, as shown in Figure 1 for HD 143275. The multiple image tiles produced by multiple observations for the same star were merged into one before spectral information was extracted. The range of number of tiles for each star was from 3 to 207, with an average of 45.

## 2.2 Step 2: Extraction of the stellar spectrum

The final merged  $2^\circ \times 2^\circ$  image tiles consist of two areas: one for the star (hereafter, the stellar area), where both the stellar and diffuse background photons coexist, and the other for the background (hereafter, the background area), where the photons from only the diffuse background are contained. We note that the diffuse background may also contain flux from unresolved fainter stars,

although we have carefully filtered out bright background pixels through the Step 1. The selection of these two areas was performed manually so that the background area was free of stellar photons of the target star. Figure 2 presents an example of the stellar area and background area selected for HD 143275.

Because the stellar area contains photons both from the star and the diffuse background, the photon counts per angstrom for the stellar area are expressed as follows:

$$F_S(\lambda) = S(\lambda) \cdot T_S + B(\lambda) \cdot T_S \cdot \Omega_S, \quad (1)$$

where  $F_S(\lambda)$  is the observed photon counts per angstrom for the stellar area (unit: photons Å $^{-1}$ ),  $S(\lambda)$  is the count rate (unit: photons s $^{-1}$  Å $^{-1}$ ) of the stellar photons to be extracted,  $T_S$  is the observation time for the stellar area (unit: s),  $B(\lambda)$  is the count rate per steradian (unit: photons s $^{-1}$  Å $^{-1}$  sr $^{-1}$ ) of the diffuse background photons to be removed from  $F_S(\lambda)$ , and  $\Omega_S$  is the celestial surface area of the stellar area (unit: steradians). Likewise, the photon counts per angstrom for the background area are expressed as follows:

$$F_B(\lambda) = B(\lambda) \cdot T_B \cdot \Omega_B, \quad (2)$$

where  $F_B(\lambda)$  is the observed photon count per angstrom for the background area (unit: photons Å $^{-1}$ ),  $T_B$  is the observation time for the background area (unit: s), and  $\Omega_B$  is the celestial surface area of the background area in units of steradians. Hence, the stellar photon count rate of  $S(\lambda)$  can be written as:

$$S(\lambda) = \frac{F_S(\lambda)}{T_S} - \frac{F_B(\lambda)}{T_B} \cdot \frac{\Omega_S}{\Omega_B}, \quad (3)$$

We verified the signal-to-noise ratio (SNR) of  $S(\lambda)$  for each star and selected only those with a wavelength-averaged SNR greater than 3.0. The total number of stars selected for spectral analysis was 532, out of approximately 4,000 stars from the *FIMS* observations that were identified through comparison with the *TDI* catalogue. Among the 532 stars, 70 stars were observed for the first time by the *FIMS*, 323 stars were observed by *IUE* with better SNRs, and the remaining 139 stars were observed by other missions, such as *UVSST* and *SKYLAB*, but with lower quality than the *FIMS*. Figure 3 indicates the locations of the 532 stars observed by *FIMS* plotted on the all-sky exposure time map.

## 2.3 Step 3: Correction of effective areas

Accurate calibration of the effective areas as a function of wavelength is necessary in order to obtain reliable stellar spectra because the detector sensitivity degrades over time. The *FIMS* observed standard stars three times for this purpose: a white dwarf G191-B2B and a B5V-type star HD 188665 were observed in December 2003, February 2004, and August 2004. These observations were compared with the reference spectra obtained previously by *HUT*, and the effective areas were obtained (Kim et al. 2004). In order to confirm these calibration results, we used the *IUE* stars and recalculated the effective areas. The *IUE* reference stars were selected according to the following criteria:

- (i) Single stars,
- (ii) Average SNR of the *FIMS* observation was greater than 7.0,
- (iii) B-type stars, in which spectrum was nearly flat without strong absorption features over the FUV wavelength range corresponding to the *FIMS* L-band, and
- (iv) Flux difference between the *IUE* and *TDI* observations was below 5%.

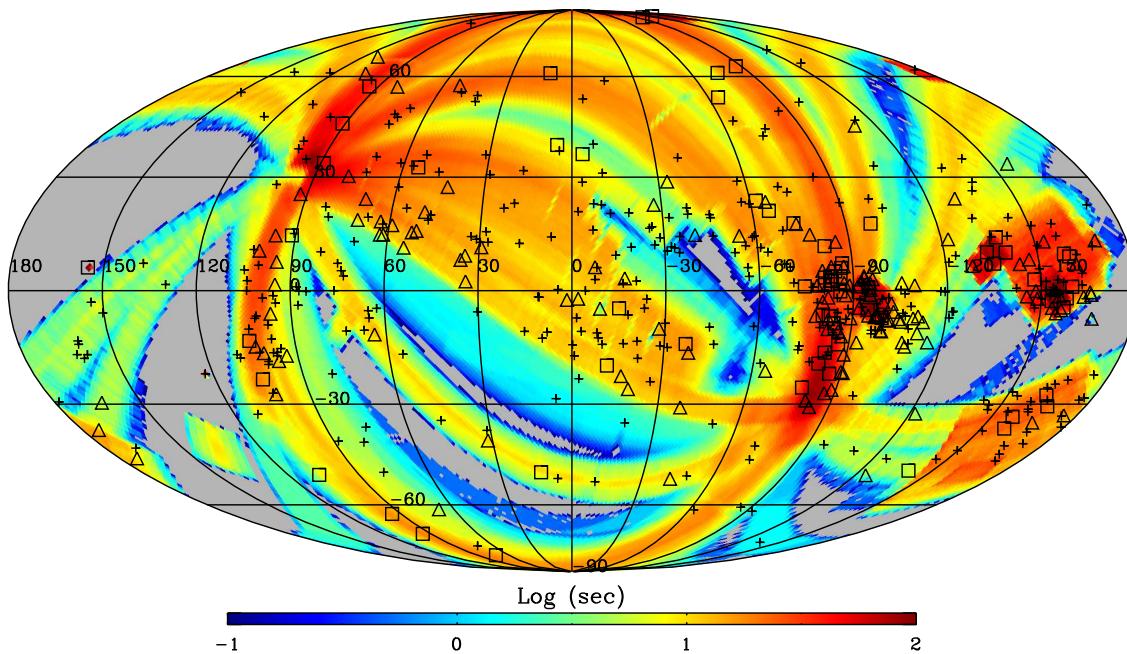


**Figure 3.** Galactic locations of the 532 stars observed by *FIMS* plotted on an all-sky exposure time map. The squares indicate the 70 stars observed for the first time by *FIMS*, and the crosses indicate the 323 stars observed by *IUE*. The remaining 139 stars are represented by triangles; these were observed in other missions such as *UVSST* and *SKYLAB*.

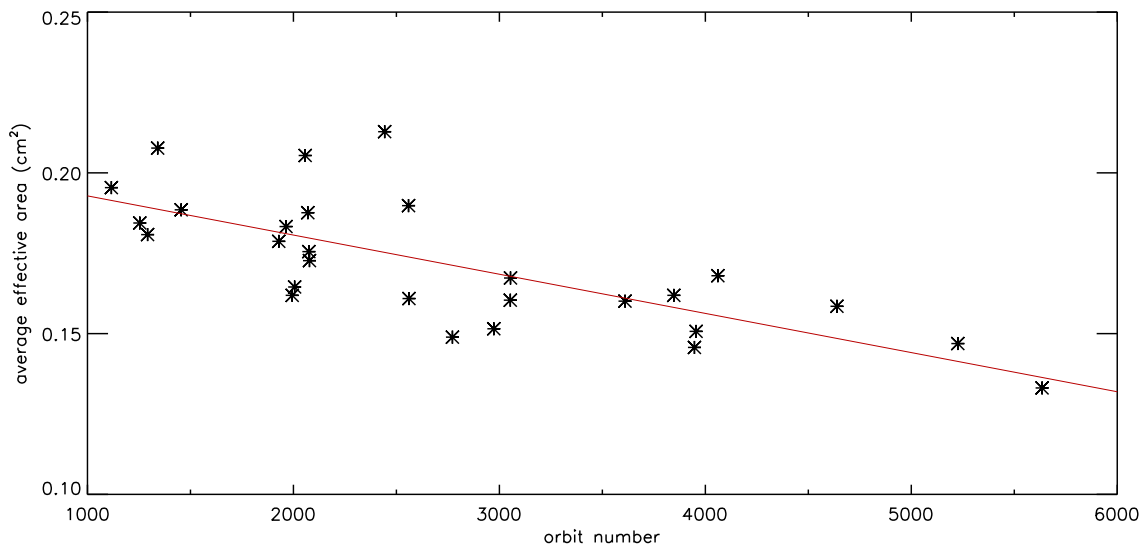


**Figure 4.** Effective areas calculated for the *IUE* reference stars listed in Table 1: they are arranged according to the orbit numbers in which the stars were observed by the *FIMS*. The solid red line is a linear fit of the data.

O-type stars were excluded because of a large number of strong absorption lines in the FUV passband, and A-type stars were also excluded because of their weak fluxes at short wavelengths. B-type stars were therefore adopted for the reference stars, though some B-type stars (especially supergiants) may still show stellar absorption lines. The New Spectral Image Processing System (NEWSIPS; Nichols & Linsky 1996) dataset of the *IUE* Final Archive, which was retrieved through the FTP site<sup>3</sup>, was used in the

present analysis. In particular, the data observed with a short wavelength camera (1150–1980 Å), taken in the observational mode with a high dispersion and large aperture, was used. A total of 28 stars were selected as the *IUE* reference stars and are listed in Table 1.

We calculated the *FIMS* effective areas for the 28 *IUE* stars by dividing the average *FIMS* photon count rates per unit wavelength (photons  $\text{s}^{-1} \text{Å}^{-1}$ ) by the average *IUE* fluxes (photons  $\text{s}^{-1} \text{cm}^{-2} \text{Å}^{-1}$ ) for the spectral range from 1370 to 1710 Å and plotted them as a function of the orbit number, which can be converted into time. Figure 4 depicts the result, which clearly shows that the *FIMS*

<sup>3</sup> <ftp://archive.stsci.edu/pub/iue/data>

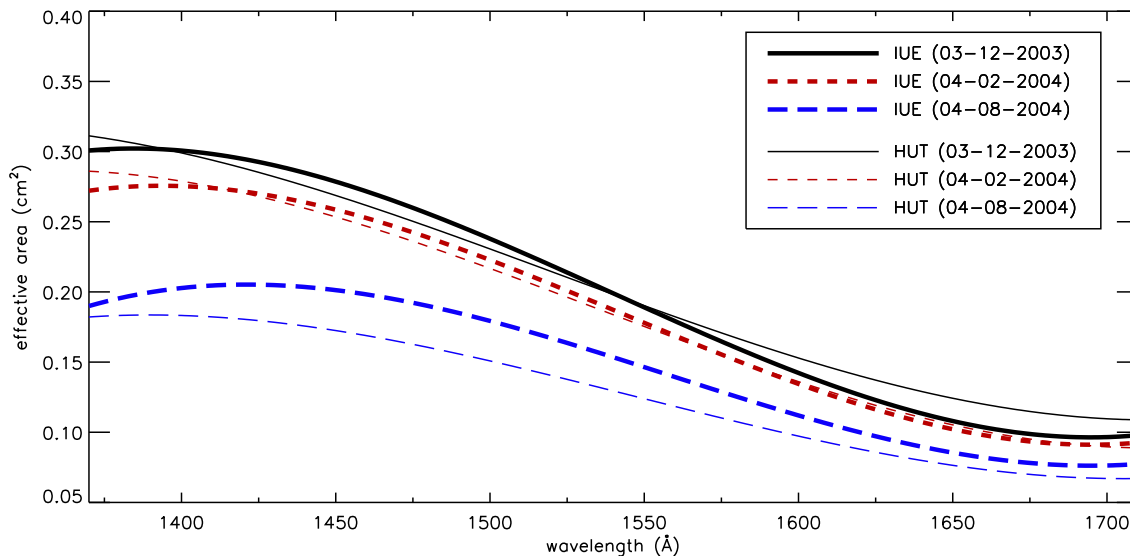


**Figure 5.** The *IUE*-based effective areas are compared with those of the previous *HUT*-based effective areas for three representative dates. The thick solid black, dashed red, and the long-dashed blue lines represent the *IUE*-based calibrations and the corresponding thin lines are the *HUT*-based calibrations, for the dates of 03-12-2003, 04-02-2004, and 04-08-2004, respectively.

effective area decreased in time. We fitted the plot using a linear function of the orbit number, as denoted by the solid red line. Figure 5 presents the final results of the effective area model for three representative orbits, which are compared with the *HUT*-based calibration. As can be seen in the figure, the *IUE*-based effective areas are in good agreement with the *HUT*-based calibration, except the one corresponding to the 4 August 2004 observation, which shows a larger effective area compared to that of the *HUT*-based calibration. However, we believe that the *IUE*-based calibration is statistically more reliable since it is based on many stars, and the *HUT*-based calibration is based on only two stars with limited observations (Kim et al. 2004). Figure 4 shows fluctuations in the estimated effective area based on the stars observed even at similar epochs, and we believe such fluctuations are the reason for the *HUT*-based curve of 4 August 2004 being lower than that based on the *IUE* stars. The fluctuations could be due to statistical variation, stellar variability, higher Earth-background, or any instrumental failure. We further confirmed the result of estimation of effective areas by comparing the calibrated *FIMS* fluxes averaged over 1370–1710 Å with the averaged *IUE* fluxes over the same wavelength band for all of the available 323 stars, as shown in Figure 6. It is seen that the two fluxes are in good agreement with each other within a 25% error for more than 92% of the stars.

### 3 RESULTS AND DISCUSSION

We present the statistics and several representative spectra of the bright stars catalogued by the *FIMS* in this section. In Figure 6, the fluxes of the *FIMS*, *TDI*-F1565, and *SKYLAB* are compared with those of the *IUE*; all are averaged in the same manner over similar wavelength ranges for 323 stars observed by the *IUE* with a large aperture mode. More than 92% of the *FIMS* fluxes, denoted by black plus (+) symbols, agree well with those of the *IUE* within the *FIMS* systemic error of 25% (Edelstein et al. 2006b). The *TDI*-F1565 fluxes, marked with red asterisk symbols, also agree well with those of *IUE* within a 25% error for 96% of the 323 stars.

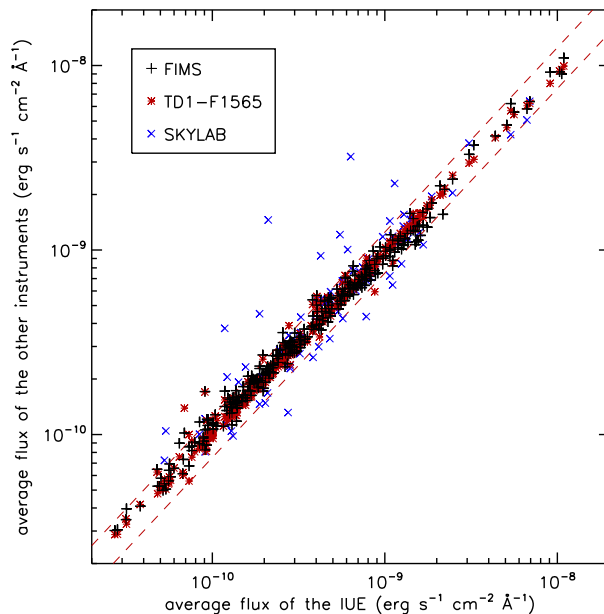


**Figure 6.** Fluxes of the *FIMS*, *TDI*-F1565, and *SKYLAB* compared with those of the *IUE*. The black plus (+), red asterisk, and blue cross (×) symbols indicate the stars observed by the *FIMS*, *TDI*, and *SKYLAB*, respectively. The two dashed red lines indicate  $\pm 25\%$  boundaries of the *IUE* flux. Both axes are log-scaled.

However, large fluctuations are seen in the *SKYLAB* fluxes, marked with blue cross (×) symbols; only 65% of 86 stars observed by *SKYLAB* show fluxes comparable to those of the *IUE* within a 25% error.

In order to verify the *FIMS* spectra after the correction of effective area, they are compared in Figure 7 with the *IUE* spectra for the 28 stars listed in Table 1, together with the available *SKYLAB* spectra. The black solid lines, dash-dotted red lines, and dashed orange lines indicate the *FIMS*, *IUE*, and *SKYLAB* spectra, respec-

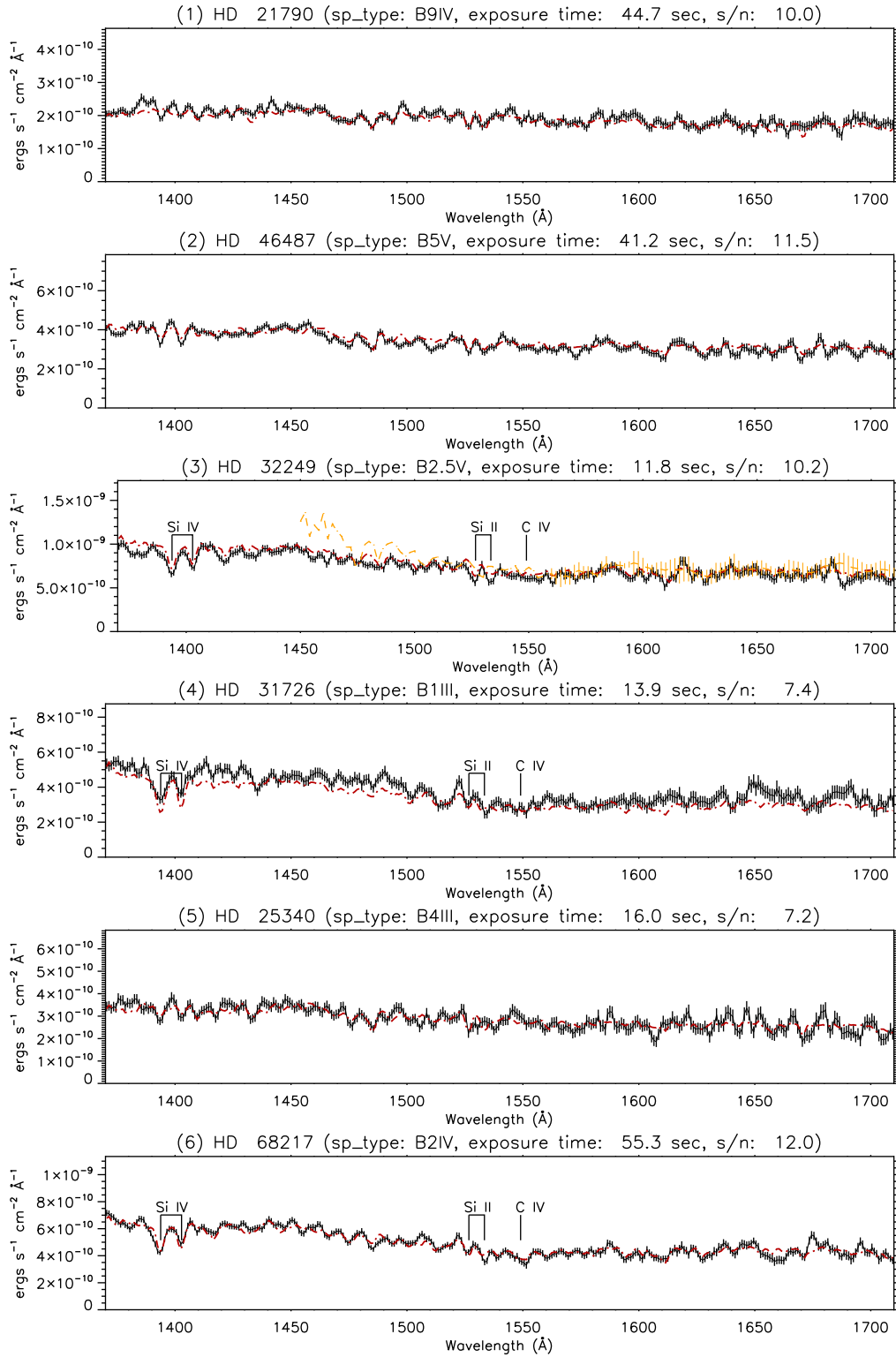


**Figure 7.** Comparison of the *FIMS* spectra with the *IUE* spectra for the 28 reference stars listed in Table 1. The solid black lines, dash-dotted red lines, and the dashed orange lines indicate the spectra observed by *FIMS*, *IUE*, and *SKYLAB*, respectively.

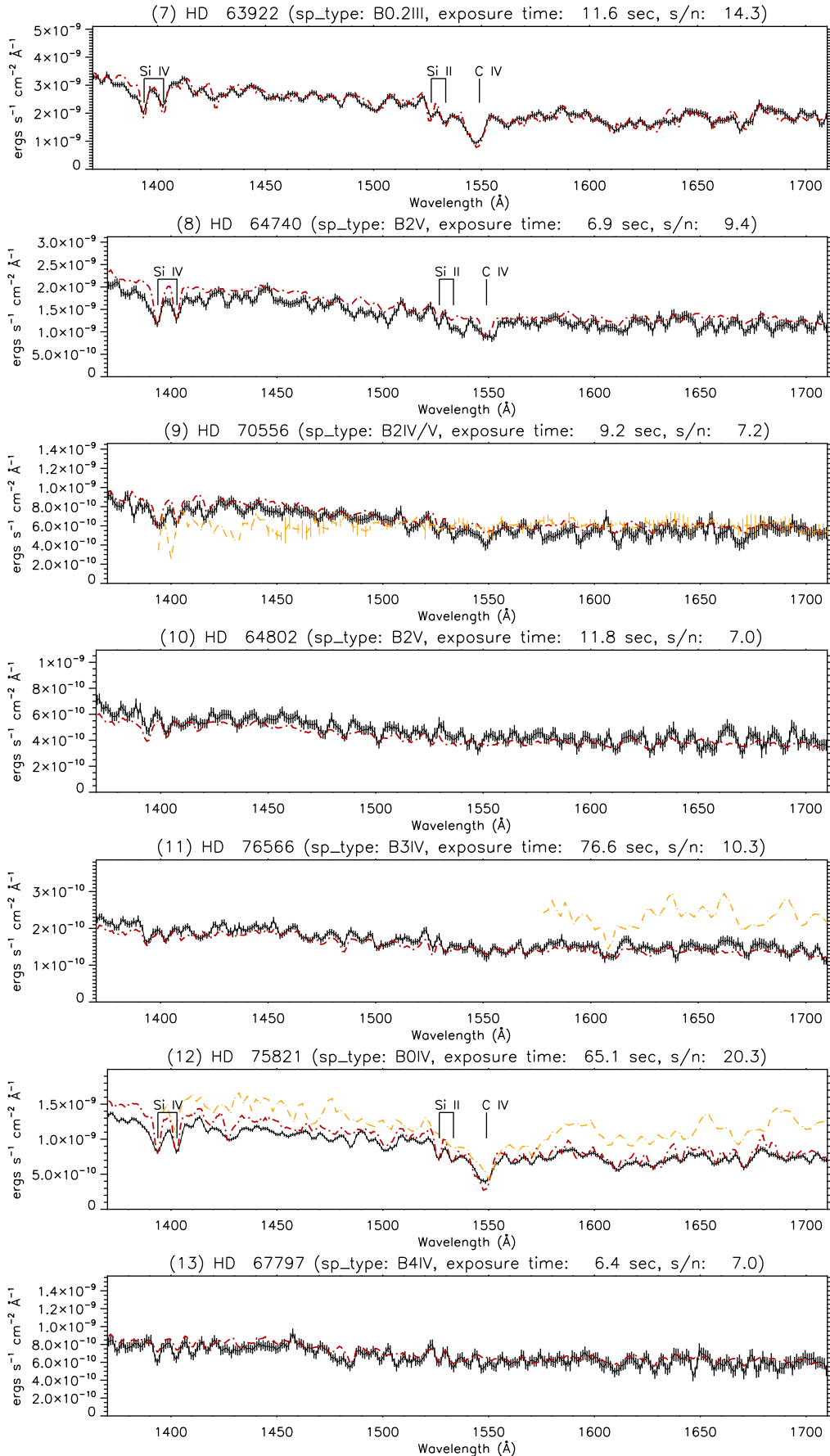


Figure 7. (cont.)

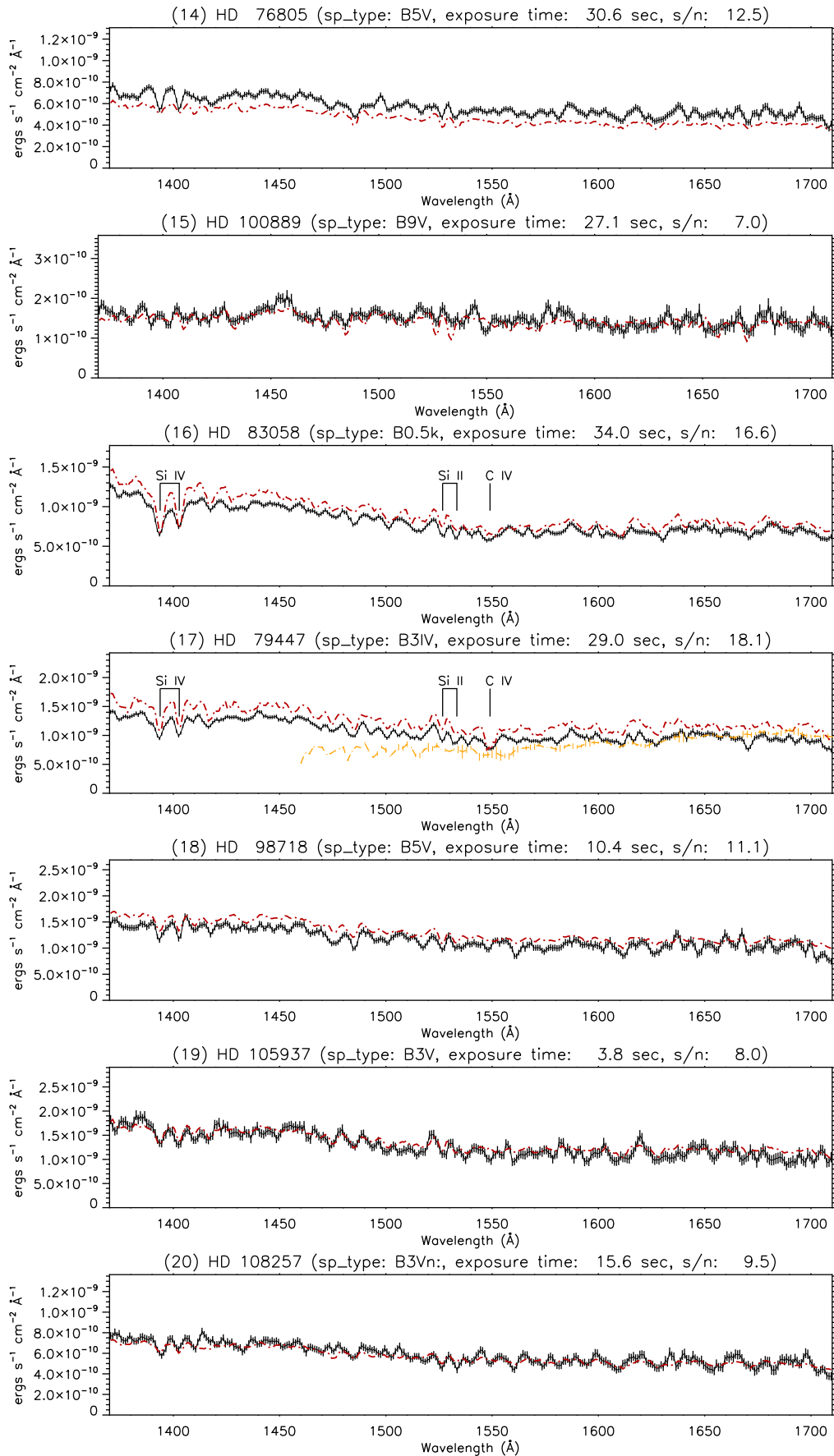


Figure 7. (cont.)



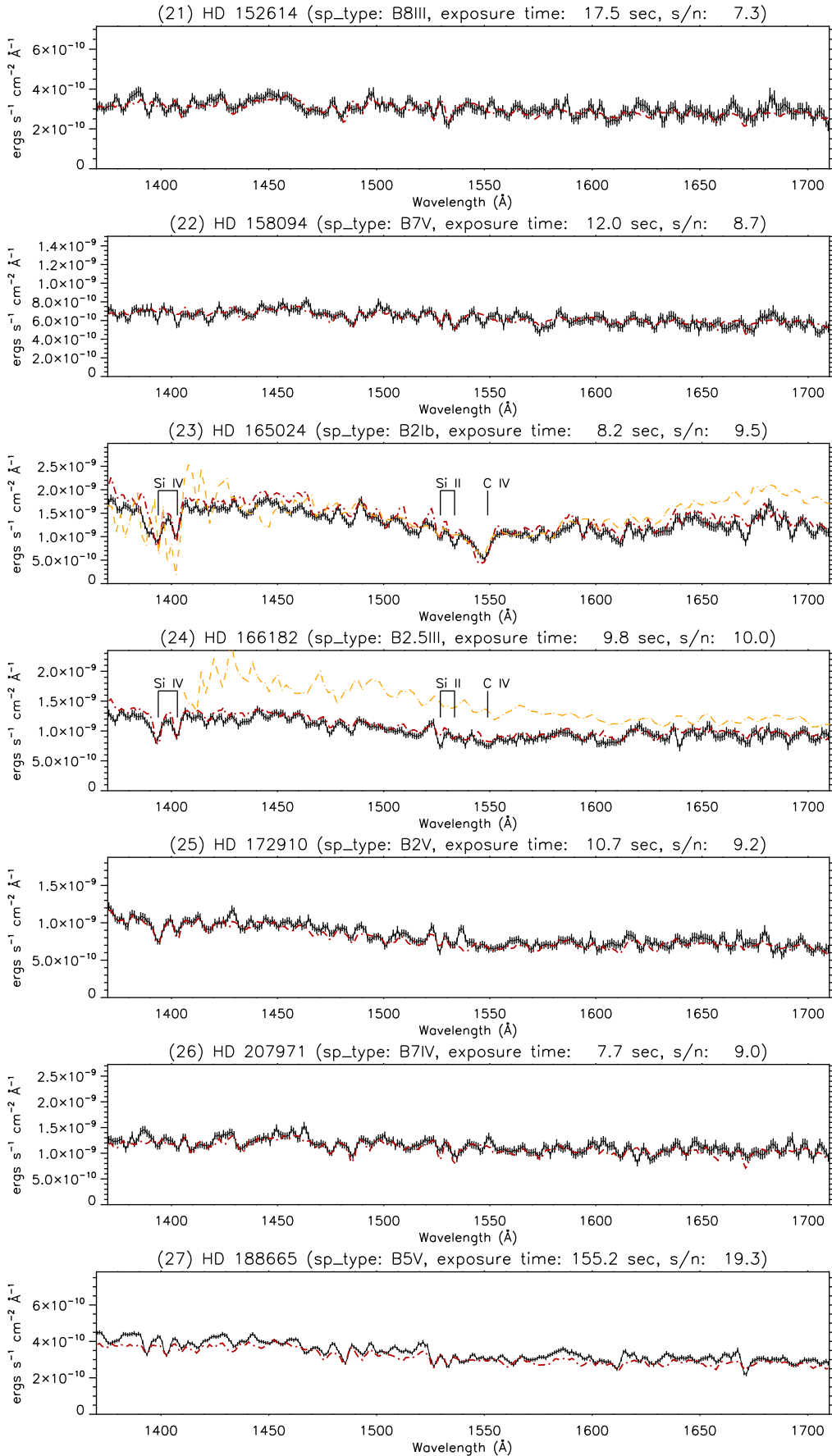


Figure 7. (cont.)

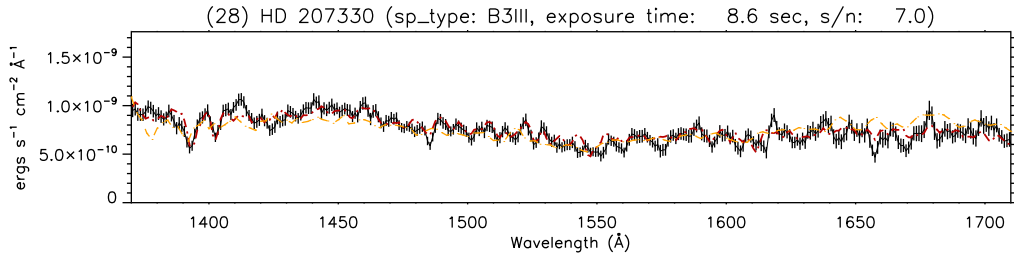


Figure 7. (cont.)

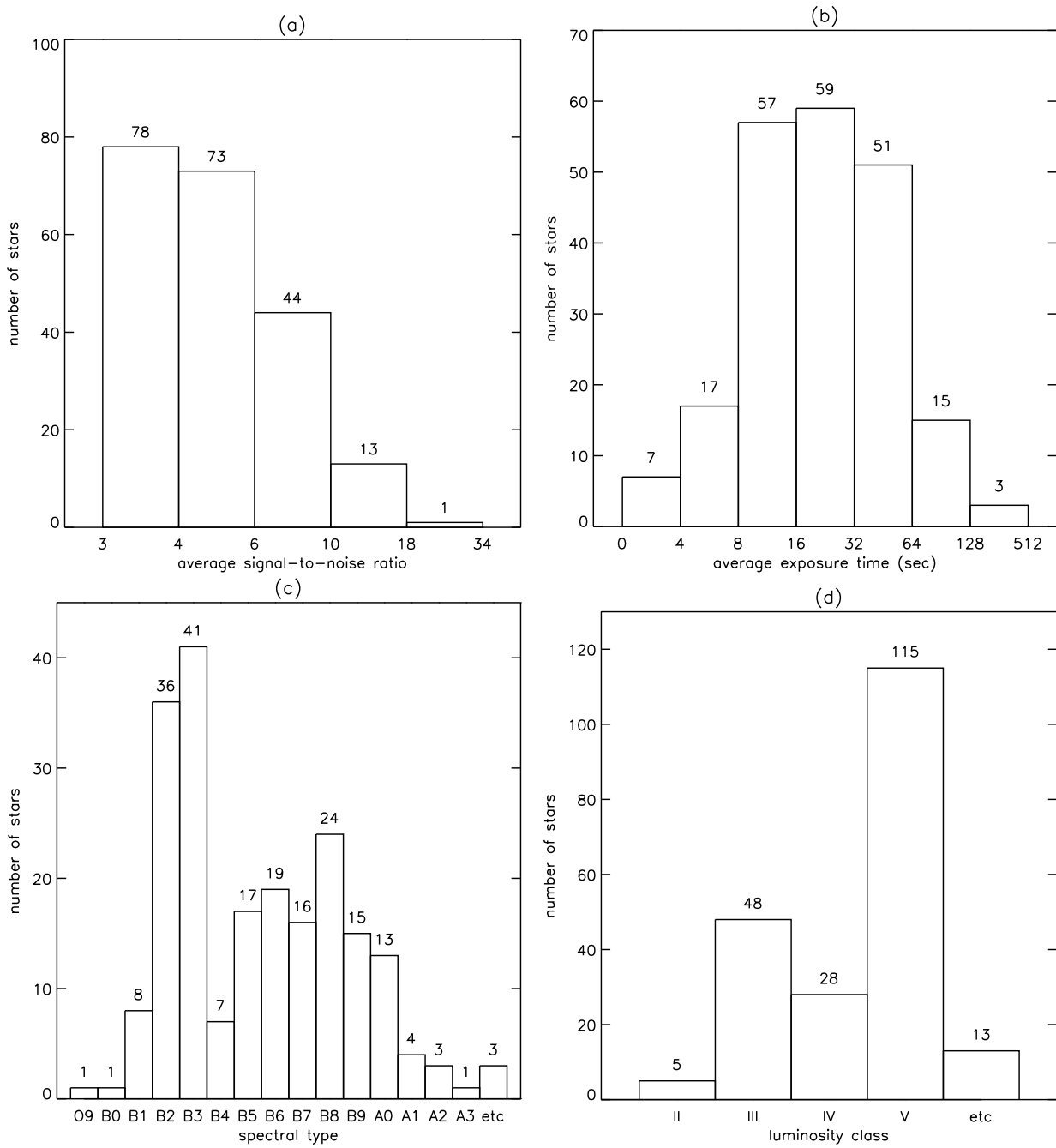


Figure 8. Statistics for the 209 *FIMS* catalogue stars indicating the number of stars against (a) the average SNR per angstrom, (b) exposure time, (c) spectral type, and (d) luminosity class.

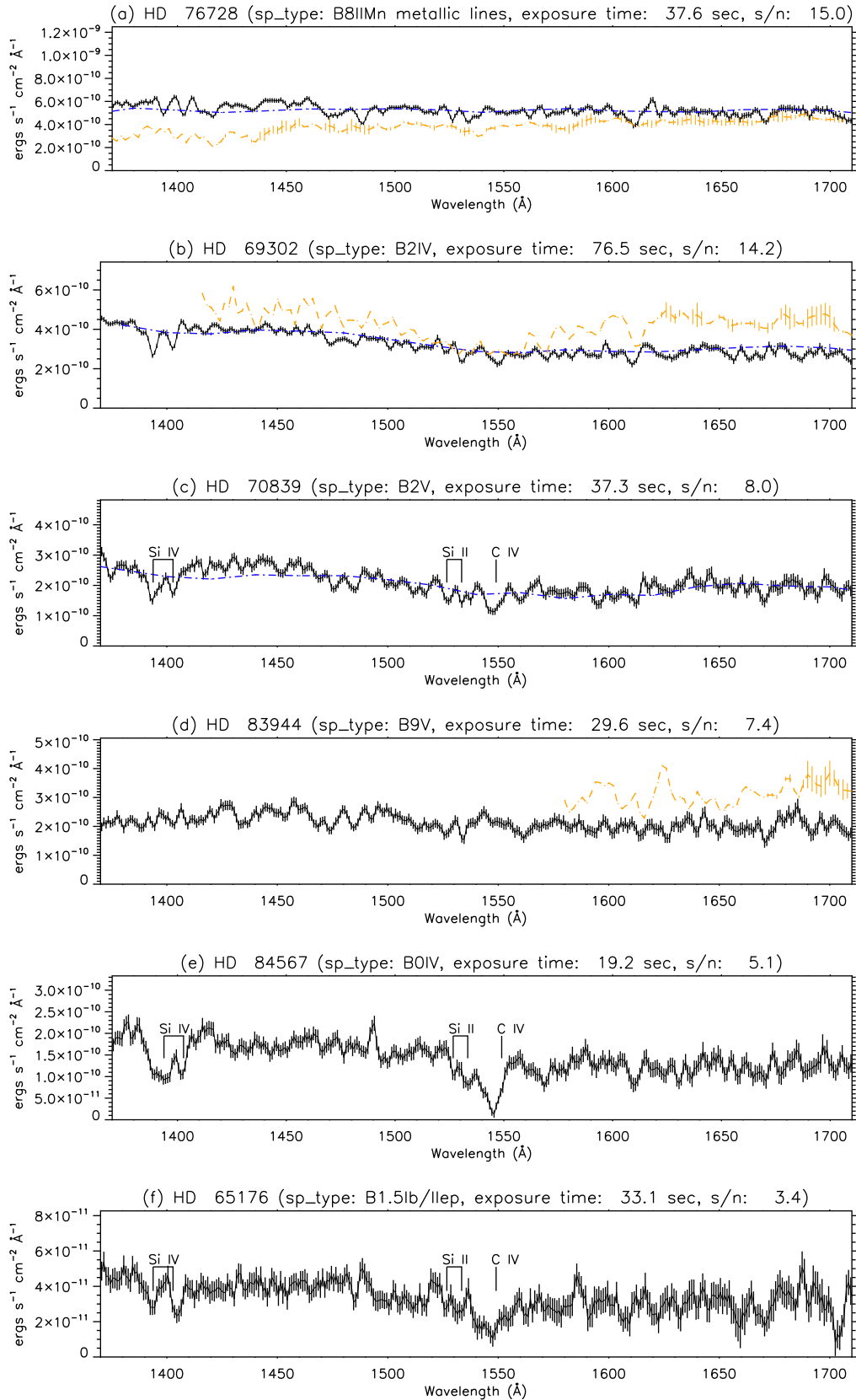
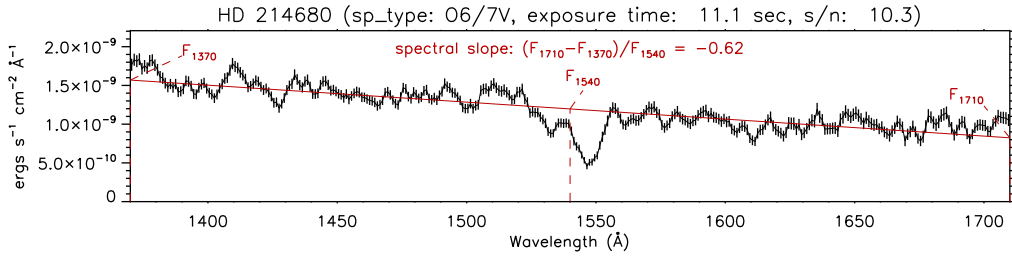


Figure 9. (a)-(f) Spectra of the sample stars listed in Table 2. The solid black line, dash-dotted blue line, and dashed orange line indicate the spectra observed by the FIMS, UVSST, and SKYLAB, respectively.

**Table 2.** List of sample stars whose spectra are presented in Figure 9.

HD ID	R.A. (deg)	Decl. (deg)	$l$ (deg)	$b$ (deg)	FIMS Flux <sup>a</sup>	FIMS S/N	FIMS Exp <sup>b</sup>	SpType (Skiff 2014)	SpType ref (Skiff 2014)	Comment
(1)	(2)	(3)	(4)	(5)	(6)	(7)	(8)	(9)	(10)	(11)
76728	133.8	-60.6	277.7	-10.0	5.15E-10	15.0	37.6	B8II	Garrison & Gray (1994)	UVSST & SKYLAB
69302	123.6	-45.8	262.0	-6.2	3.17E-10	14.2	76.5	B2IV	Houk (1978)	UVSST & SKYLAB
70839	125.3	-58.0	272.9	-11.9	2.04E-10	8.0	37.3	B2V	Cucchiaro et al. (1976)	UVSST
83944	144.8	-61.3	281.9	-6.6	2.10E-10	7.4	29.6	B9V	Zorec et al. (2009)	SKYLAB
84567	146.3	-30.2	261.8	17.5	1.38E-10	5.1	19.2	B0IV	Houk (1982)	FIMS only
65176	119.4	-1.6	222.1	13.9	3.29E-11	3.4	33.1	B1.5Ib/Iep	Schmidt-Kaler (1967)	FIMS only

<sup>a</sup> units:  $\text{erg s}^{-1} \text{cm}^{-2} \text{\AA}^{-1}$ <sup>b</sup> units: sec**Figure 10.** Linear fit of the spectrum of HD 214680.

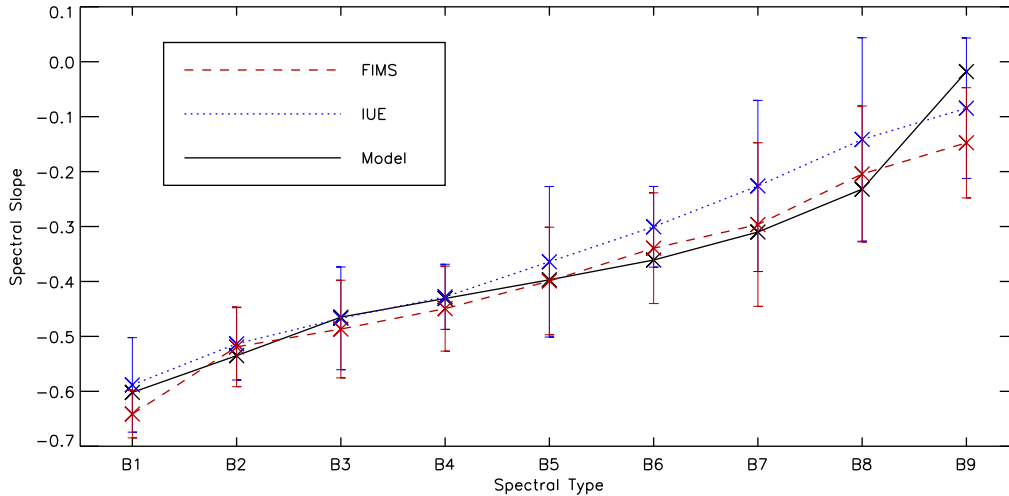
tively. The *FIMS* spectra are seen to match well with the corresponding *IUE* spectra. For some stars, such as (14) HD 76805, (16) HD 83058, (17) HD 79447, and (18) HD 98718, the flux levels between the *FIMS* and the *IUE* observations show discrepancies due to the fluctuation in the effective area but they are all within 25% of the *FIMS* systematic error range (Edelstein et al. 2006b). The prominent absorption lines of early-type stars, such as C IV  $\lambda\lambda 1548, 1551$  and Si IV  $\lambda\lambda 1394, 1403$  features, are clearly seen in the *FIMS* spectra. However, narrower lines, such as Si II\*  $\lambda\lambda 1527, 1533$ , are less clear in the *FIMS* spectra than in the *IUE* spectra because of the variation of spectral resolution across the detector. The *SKYLAB* spectra show large deviation from the corresponding *IUE* and *FIMS* spectra. This demonstrates the superior quality of *FIMS* data compared to those of *SKYLAB*.

Figure 8 presents statistics for the 209 stars of the *FIMS* catalogue, excluding those observed by the *IUE*. Figures 8(a) to 8(d) are histograms of the average SNR per angstrom, exposure time, spectral type, and luminosity class, respectively. The figures illustrate that, of the 209 catalogue stars, the spectra of 58 stars had high SNRs above 6.0. Most of these were bright stars observed with longer exposure times than the average of 20 s. The stellar spectral type of catalogue stars ranged from O9 to A3; 115 of these stars are main sequence stars, 28 are subgiant stars, 48 are normal giant stars, 5 are bright giant stars, and 13 are unknown. The stars with spectral types beyond A4 were not analysed with a sufficient SNR because their flux level was weak in the FUV band due to the low surface temperature; hence, they have been excluded from the catalogue.

For the stars listed in Table 2, example spectra are plotted in Figure 9 in order to compare the *FIMS* spectra with the previous observations of *UVSST* and *SKYLAB*. The example spectra were arbitrarily chosen and displayed in decreasing order of SNR to show variation of the spectral quality. The *FIMS* spectra are indicated using solid black lines in the figure. It is seen that the *UVSST* spectra,

marked with dash-dotted blue lines in Figures 9(a) to 9(c) agree well with the *FIMS* spectra; however, the absorption features are not resolved in the *UVSST* spectra due to the low spectral resolution of 35 Å. The *SKYLAB* spectra, which are marked using dashed orange lines in Figures 9(a), 9(b), and 9(d), have a similar spectral resolution to that of the *FIMS* spectra. However, as seen in Figure 6, the flux levels of the *SKYLAB* spectra deviate significantly from those of the *IUE* spectra while the *FIMS* flux levels are more or less consistent with the *IUE* observations. Hence, we believe that the *FIMS* spectra are more reliable than the *SKYLAB* spectra. Figures 9(e) and 9(f) show two examples observed by the *FIMS* only. Strong absorption lines including Si IV, Si II\*, and C IV lines are seen in both spectra even though the SNR is low in the case of Figure 9(f). According to the SIMBAD database, the spectral type of HD 65176, shown in Figure 9(f), is A0. It should be noted that the corresponding spectrum of A0 is not expected to have such prominent absorption features in the Si IV and C IV lines. We will discuss this discrepancy in the following text.

Finally, we would like to discuss possible applications of the *FIMS* catalogue. The FUV wavelength band covered by the *FIMS* includes many ion lines associated with hot and warm gases. Hence, as can be seen in Figure 9, the prominent ion absorption lines such as C IV  $\lambda\lambda 1548, 1551$  and Si IV  $\lambda\lambda 1394, 1403$  can be used to confirm the spectral classes for early-type stars. For instance, strong Si IV absorption features shown in Figure 9(e) indicate that HD 84567 is a supergiant or giant star with a higher mass-loss rate rather than a subgiant (see Bianchi & Garcia 2002). On the other hand, the measured slope (-0.67) after reddening correction is consistent with -0.66 estimated from the Skiff's spectral type of B0IV. Another example is HD 65176, which is classified to be A0 in the SIMBAD database. However, the deep absorption features shown in Figure 9(f) suggest that the star is an early B-type



**Figure 11.** Variation of the spectral slopes in the FUV passband for the stellar spectral type from B1 to B9. The dashed red, dotted blue, and solid black lines indicate the spectral slope variations for the *FIMS*, the *IUE*, and the Castelli & Kurucz model (Castelli & Kurucz 2003) spectra, respectively.

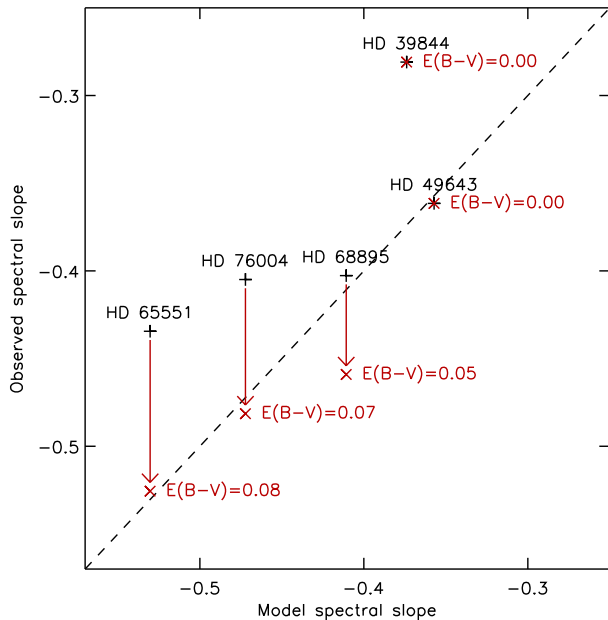


**Figure 12.** Comparison of spectral slopes between observations and models for several example stars. The black plus (+) symbols indicate the spectral slopes before reddening correction, and the red cross (x) symbols indicate those after correction. The dashed black line indicates the one-to-one correspondence between the observation and model spectral slopes.

as assigned to be B1.5Ib/IIep in Skiff (2014)<sup>4</sup>. Furthermore, we note that the spectral shape changes significantly in this wavelength band as the spectral type changes for the early-type stars. We, therefore, used the spectral classification of Skiff (2014) in this paper. As discussed below, this property can be used to confirm or identify the spectral classes and even estimate the interstellar extinction in UV wavelengths (e.g., the FUV rise; Fitzpatrick & Massa 1988), which cannot be inferred from optical and near infrared observations, if the spectral type of the target star is correctly identified because the

interstellar extinction is strongly wavelength-dependent over this wavelength range.

First, let us define the spectral slope. The spectral slope is calculated from a linear fit over the whole wavelength range from 1370 Å to 1710 Å, as shown in Figure 10 for the example star, HD 214680. It is defined as follows:

$$\text{spectral slope} = (F_{1710} - F_{1370})/F_{1540}, \quad (4)$$

where  $F_{1710}$ ,  $F_{1370}$ , and  $F_{1540}$  are the flux values obtained from the linear fit at wavelengths of 1710, 1370, and 1540 Å, respectively. We obtained the average spectral slope for each stellar spectral type based on the Skiff (2014) from B1 to B9 with  $\sim 20$  stars for each spectral type. The  $E(B-V)$  colour excess was estimated using the intrinsic colour index  $(B-V)_0$  of Fitzgerald (1970) and the observed colour index  $(B-V)$  of the SIMBAD database. We selected only those stars with colour excess  $E(B-V) < 0.05$ , corresponding to an optical depth of 0.35 at 1540 Å, and performed reddening correction using the colour excess. The extinction law was adopted from Weingartner & Draine (2001) with  $R_V = 3.1$ . We compared the spectral slopes estimated from the *FIMS* to those of the *IUE* and a stellar synthetic model. The theoretical model spectra were calculated through interpolation on a grid of the Kurucz model (Castelli & Kurucz 2003) using the effective temperature and gravity calibration given in Straižys & Kuriliene (1981). Figure 11 shows the results of the spectral slopes. The three spectral slopes estimated from the *FIMS*, *IUE*, and a theoretical model are in good agreement, indicating that the spectral slope is steeper in earlier spectral types, as expected. The statistical errors, especially the large ones, may stem from the misidentification of the spectral type. The sub-classification of the spectral type contributes in part to the error. A large source of the uncertainty would be the SIMBAD's photometry and colors. There are additional sources of uncertainty to the spectral slope. We assumed a constant  $R_V$ , which in fact varies from a sightline to sightline, in performing reddening correction. Another non-negligible source might be the uncertainty in the calibration of the effective temperature and gravity. The calibration used in this paper is based on evolutionary models and thereby subject to their intrinsic errors (e.g., Herrero et al. 1992).

Figure 12 shows some examples of how the spectral slopes in Figure 11 can be used for the identification of the spectral type. In

<sup>4</sup> <http://vizier.u-strasbg.fr/viz-bin/VizieR?-source=B/MK>

Figure 12, the black plus (+) symbols indicate the spectral slopes before reddening correction and the red cross (×) symbols indicate those after correction. The sources in the figure were arbitrarily chosen. We see that the spectral slopes of HD 65551, HD 76004 and HD 49643 are consistent with the model spectral slopes when the reddening correction is taken into account. On the other hand, the spectral slopes of HD 68895 and HD 39844 are very different from the corresponding model spectral slopes. The spectral slope of HD 68895 after correction, estimated from the *FIMS* spectrum, is -0.46 while the model spectral slope corresponding to the spectral type of B5V (Houk 1978) is -0.41. This spectral slope of -0.46 is more consistent with B3V (Cucchiario et al. 1976) or B4V than B5V if the reddening correction is correct. If the spectral type of B5V is correct, the colour excess need to be changed to  $E(B-V)=0.01$ , or  $R_V$  should be larger than 3.1. In the same way, the spectral slope of HD 39844 indicates that its spectral type is more consistent with B7V or B8V than with the spectral type of B6V (Cucchiario et al. 1977) if the interstellar extinction is negligible. On the other hand, if the spectral type of B6V is correct, the colour excess needs to be changed to  $E(B-V)=0.08$ , or  $R_V$  should be smaller than 3.1 for  $E(B-V)$  to be less than 0.08.

#### 4 CONCLUDING REMARKS

We extracted the *L*-band (1370–1710 Å) spectra for 532 stars observed using the *FIMS* during its mission lifetime of one and a half years, which covered approximately 84% of the sky. Of these stars, 323 were also observed by the *IUE* with higher signal-to-noise ratios than the *FIMS*; hence, these data were used to validate the *FIMS* spectra. The remaining 209 stars were compiled as a catalogue: 70 stars were observed by the *FIMS* for the first time and 139 stars were observed previously by *UVSST* and/or *SKYLAB*. We included these 139 stars in the catalogue because we believe the *FIMS* spectra provide better spectral resolution and/or higher reliability than the previous observations. The catalog contains only the stars whose spectra meet the criterion of average SNRs per angstrom higher than 3.0. The full spectra of the 209 catalogue stars observed by the *FIMS* can be downloaded from the KASI website<sup>5</sup>.

#### ACKNOWLEDGMENTS

*FIMS/SPEAR* is a joint project of KAIST (Korea), KASI (Korea), and UC Berkeley (USA), funded by the Korean MOST and NASA (grant NAG5-5355). K.-W. Min acknowledges the support by the National Research Foundation of Korea through its Grant No. NRF 2012M1A3A4 A01056418.

#### REFERENCES

Abt H. A., Cardona O. 1983, *ApJ*, 272, 182  
 Ayres T. R. 2010, *ApJS*, 187, 149  
 Bertone E., Chavez M. 2011, *Ap&SS*, 335, 69  
 Bianchi L., Garcia M. 2002, *ApJ*, 581, 610  
 Boggess A. et al. 1978, *Nature*, 275, 372  
 Boksenberg A. et al. 1973, *MNRAS*, 163, 291  
 Brandt J. C. et al. 1994, *PASP*, 106, 890

Castelli F., Kurucz R. L. 2003 (IAU Symposium 210, Modelling of Stellar Atmospheres, Uppsala, Sweden, eds. N.E. Piskunov, W.W. Weiss, and D.F. Gray, 2003, ASP-S210)  
 Cucchiario A., Jaschek M., Jaschek C., Macau-Hercot D. 1976, *A&AS*, 26, 241  
 Cucchiario A., Macau-Hercot D., Jaschek M., Jaschek C. 1977, *A&AS*, 30, 71  
 Davidsen A. F. et al. 1992, *ApJ*, 392, 264  
 Edelstein J. et al. 2006a, *APJL*, 644, L153  
 Edelstein J. et al. 2006b, *APJL*, 644, L159  
 Fitzgerald M. P. 1970, *A&A*, 4, 234  
 Fitzpatrick E. L., Massa D. 1988, *ApJ*, 328, 734  
 Garrison R. F., Gray R. O. 1994, *AJ*, 107, 1556  
 Gorski K. M., Hivon E., Banday A. J., Wandelt B. D., Hansen F. K., Reinecke M., Bartelmann M. 2005, *APJ*, 622, 759  
 Green J. C. et al. 2012, *ApJ*, 774, 1  
 Henize K. G., Wray J. D., Parsons S. B., Benedict G. F., Bruhweiler F. C., Rybski P. M., O’Callaghan F. G. 1975, *APJL*, 199, L119  
 Henize K. G., Wray J. D., Parsons S. B., Benedict G. F. 1979, Catalog of Far-Ultraviolet Objective-Prism Spectrophotometry: SKYLAB Experiment S-019, Ultraviolet Stellar Astronomy (NASA Ref. Publ. 1031; Washington: NASA)  
 Herrero A., Kudritzki R. P., Vilchez J. M., Kunze D., Butler K., Haser S. 1992, *A&A*, 261, 209  
 Hill P. W., Lynas-Gray A. E. 1977, *MNRAS*, 180, 691  
 Houk N. 1978, Michigan Catalogue of Two-Dimensional Spectral Types for the HD Stars. Volume 2. (Ann Arbor, MI: Univ. Michigan Press)  
 Houk N. 1982, Michigan Catalogue of Two-Dimensional Spectral Types for the HD Stars. Volume 3. (Ann Arbor, MI: Univ. Michigan Press)  
 Humphries C. M., Jamar C., Malaise D., Wroe H. 1976, *A&A*, 49, 389  
 Jamar C., Macau-Hercot D., Monfils A., Thompson G. I., Houziaux L., Wilson R. 1976, Ultraviolet Bright Star Spectrophotometric Catalogue (ESA Special Report 27; Paris: ESA)  
 Jenkins E. B., Reale M.A., Zucchino P.M., Sofia U.J., 1996, *Ap&SS*, 239, 315  
 Kim I.-J., Seon K.-I., Yuk I.-S., Nam U.-W., Jin H., Park J.-H. 2004, *JASS*, 21, 383 (*JASS: Journal of Astronomy and Space Science*)  
 Korpela E. J. et al. 2006, *APJL*, 644, L163  
 Kruk J. W., Durrance S. T., Kriss G. A., Davidsen A. F., Blair W. P., Espey B.R., Finley D. S. 2006, *APJL*, 454, L1  
 Moos H.W. et al. 2000, *ApJL*, 538, L1  
 Morrissey P. et al. 2007, *ApJS*, 173, 682  
 Nichols J. S., Linsky J. L. 1996, *AJ*, 111, 517  
 Reed, B. C. 2003, *AJ*, 125, 2531  
 Rogerson J. B., Spitzer L., Drake J. F., Dressler K., Jenkins E.B., Morton D.C., York D.G. 1973, *ApJL*, 181, L97  
 Sahnou D. J. et al. 2000, *ApJL*, 538, L7  
 Schmidt-Kaler T. 1967, *PASP*, 79, 181  
 Skiff B. A. 2014, *VizieR Online Data Catalog*, 1, 2023  
 Snow T. P., Jr., Jenkins E. B. 1977, *ApJS*, 33, 269  
 Straižys V., Kuriliene G. 1981, *Ap&SS*, 80, 353  
 Thompson G. I., Nandy K., Jamar C., Monfils A., Houziaux L., Carnochan D. J., Wilson R. 1978, Catalogue of Stellar Ultraviolet Fluxes (TD1): A Compilation of Absolute Stellar Fluxes Measured by the Sky Survey Telescope (S2/68) Aboard the ESRO Satellite TD-1 (London: The Science Research Council)  
 Weingartner J. C., Draine B. T. 2001, *ApJ*, 548, 296

<sup>5</sup> <http://ysjo.kasi.re.kr>

Woodgate B. E. et al. 1998, PASP, 110, 1183  
Zorec J., Cidale L., Arias M. L., Fremat Y., Muratore M. F., Torres  
A. F., Martayan C. 2009, A&A, 501, 297

This paper has been typeset from a  $\text{\TeX}$ / $\text{\LaTeX}$  file prepared by the author.